

WAKE DYNAMICS IN THE LOWER BRANCH AND DESYNCHRONIZATION REGIONS OF 1DOF VIV

Graham Riches

Dept. of Mechanical and Manufacturing Engineering
University of Calgary
2500 University Dr NW, Calgary, AB T2N 1N4
gpriches@ucalgary.ca

Chris Morton

Dept. of Mechanical and Manufacturing Engineering
University of Calgary
2500 University Dr NW, Calgary, AB T2N 1N4
chris.morton@ucalgary.ca

ABSTRACT

Vortex induced vibrations of a circular cylinder has been investigated experimentally using a cyber-physical apparatus with $m^* = 8$ and $\zeta = 0.005$. The Reynolds number is held fixed at $Re = 4000$, with the reduced velocity being modified via a change in the structural natural frequency in a cyber-physical controller. A detailed analysis of lower branch and desynchronization regions of VIV is presented through Proper Orthogonal Decomposition and Phase Averaging. An alternative methodology for extracting coherent motions from the wake flow is proposed by performing a POD analysis on the residual error field of the phase-averaged flow. The results demonstrate that coherent motions of the cylinder wake can either provide damping or excitation to the cylinder motion, and this is captured within the third most energetic POD mode.

INTRODUCTION

Vortex induced vibrations of circular cylinders has been studied extensively for well over a century (e.g., Feng (1968), Brika & Laneville (1993), Sarpkaya (2004), Morse & Williamson (2009)). It is a fluid-structure interaction problem which has provided engineering challenges to the design civil structures (e.g., cable-tensioned bridges) as well as mechanical engineering devices (e.g., heat exchangers). A comprehensive review of VIV can be found in the works of Sarpkaya (2004).

The main parameters of interest in VIV include the response amplitude ($A^* = A/D$) and frequency ($f^* = f/f_N$), the reduced velocity ($U^* = U_\infty/f_N D$), the mass ratio ($m^* = 4m/\rho\pi D^2 L$) and the damping ratio ($\zeta = c/2\sqrt{km}$). The VIV response for a low mass-damping system across a range of reduced velocities, is characterized by four distinct response branches: (i) initial branch, where the cylinder vortex shedding frequency (f_{VS}) begins to approach the natural frequency (f_N) of the system causing an increase in the amplitude of oscillations. Here, the oscillation occurs at the superposition of two frequencies (f_N and f_{VS}). (ii) upper branch, when the response amplitude of the cylinder transi-

tions to a higher state, and the oscillation frequency differs from the vortex shedding frequency and begins to follow the natural frequency ($f^* \approx 1$). (iii) lower branch, where the amplitude response of the cylinder transitions to a lower amplitude steady oscillation whose frequency is locked-in slightly above the system natural frequency. This 'lock-in' behaviour occurs when the motion of the cylinder has become synchronized to the interaction in the separated shear layers which induce vortex shedding (Sarpkaya, 2004). (iv) desynchronization, where the vortex shedding and cylinder motion can no longer remain synchronized and the response of the cylinder decays. Here, desynchronization implies that no vortex wake pattern is synchronized to the cylinder motion.

While extensive analysis of VIV wake shedding modes has been carried out by Morse & Williamson (2009) and others, no efforts have been made to date to classify the wake patterns persisting within the transition region between the lower branch and desynchronization regions, as well as within the desynchronization region. Elucidating this behavior can provide added insight into the desynchronization process, which is the main objective of the present work.

METHODOLOGY

Experiments were carried out in a Water Tunnel Facility at the University of Calgary. A cyber-physical apparatus (Figure 1a) was employed to study VIV of a circular cylinder. The parameters investigated within this study correspond to $m^* = 8$, $\zeta = 0.005$, $Re = 4000$, and $3 < U^* < 11$. The reduced velocity was modified via a change in the structural natural frequency in the cyber-physical controller shown in Figure 1b in the Laplace domain.

The total transverse force on the circular cylinder was measured with an ATI Mini40 force transducer with a resolution of $0.005[N]$. The motion of the cylinder is driven by a ClearPath digital brushless servomotor (MCVC-2341P) through a timing belt system with negligible backlash. The position of the traverse is measured using an Omron opti-

cal encoder yielding a position resolution of $0.0375[mm]$. The position and force signals are measured in real-time at $1[kHz]$ via an Advantech PCI1716L data acquisition card. Further details of the cyber-physical system can be found in Riches & Morton (2018) and (Riches, 2018).

Time-resolved two-component planar Particle Image Velocimetry (PIV) data were obtained for select cases. The imaging system employed a high speed Phantom Miro M340 digital camera focused on a plane located at the cylinders mid-span and illuminated by a laser sheet generated from a Photonics 20mJ Nd:YLF high repetition rate pulsed laser with a wavelength of $\lambda = 527[nm]$. PIV images were processed using *LaVision DaVis 8.3* software to produce time-resolved velocity fields. Uncertainties for the velocity vectors were calculated using correlation statistics method employed within *DaVis 8.3* (2.2% in the free stream and 4.0% in the wake, on average).

The raw PIV images are post-processed through three methods: (i) phase-averaging based on the cylinder position, (ii) POD analysis and low order model reconstruction, and (iii) a combination of (i) and (ii). To describe the each of the post-processing methods requires an understanding of POD.

Using the traditional Reynolds decomposition, the velocity field in a turbulent wake $u_i(\mathbf{x}, t)$ can be represented in Cartesian tensor notation by the summation of the mean $U_i(\mathbf{x})$, and a time-dependant fluctuating flow $u'_i(\mathbf{x}, t)$ as

$$u_i(\mathbf{x}, t) = U_i(\mathbf{x}) + u'_i(\mathbf{x}, t). \quad (1)$$

The Reynolds stresses result from the application of the Reynolds decomposition and averaging of the Navier-Stokes equations. The fluctuating (turbulent) kinetic energy k is represented as

$$\overline{q^2} = 1/2(\overline{u'^2} + \overline{v'^2}), \quad (2)$$

which is the two-dimensional (2D) contribution to k where u' and v' represent the physical components of the fluctuating velocity corresponding to the Cartesian indices $i = 1, 2$. The production of k in a 2D mean wake is:

$$G_k = \left(\overline{v'^2} - \overline{u'^2} \right) \frac{\partial U}{\partial x} - \overline{u'v'} \left(\frac{\partial V}{\partial x} + \frac{\partial U}{\partial y} \right), \quad (3)$$

which explicitly groups the contributions of the normal and shear Reynolds stresses to the production term of the k transport equation. Note that this is exact since $\partial U / \partial x = -\partial V / \partial y$ for a mean 2D flow and thus $w'^2 \partial W / \partial z = 0$. The total TKE contained in the PIV domain Ω is given as

$$TKE = \iint_{\Omega} kdA \approx \iint_{\Omega} \overline{q^2} dA. \quad (4)$$

Following Reynolds & Hussain (1972), the flow can be further decomposed by splitting the fluctuating field into coherent motions $u_{ci}(\mathbf{x}, t)$ and the remaining incoherent turbulent motions $u''_i(\mathbf{x}, t)$ yielding the triple-decomposition:

$$u_i(\mathbf{x}, t) = U_i(\mathbf{x}) + u_{ci}(\mathbf{x}, t) + u''_i(\mathbf{x}, t). \quad (5)$$

Using the snapshot POD method of Sirovich (1987), the time-varying velocity field $u'_i(\mathbf{x}, t)$ is decomposed into a finite sum of spatial eigenfunctions $\phi_k(\mathbf{x})$ multiplied by a time-dependent temporal modal coefficient $a_k(t)$:

$$\mathbf{u}'(\mathbf{x}, t) = \sum_{k=1}^N \phi_k(\mathbf{x}) a_k(t), \quad (6)$$

where \mathbf{u}' is the vector representation of the components u'_i . $\phi_k(\mathbf{x})$ satisfy the orthonormality condition, where the inner-product is defined as

$$(\phi_i(\mathbf{x}), \phi_j(\mathbf{x})) = \iint_{\Omega} \phi_i(\mathbf{x}) \cdot \phi_j(\mathbf{x}) dA = \delta_{ij}, \quad (7)$$

with

$$a_k(t) = (\mathbf{u}', \phi(\mathbf{x})), \quad (8)$$

where the modes are ranked by descending energetic content ($\lambda_1 > \lambda_2 > \dots > \lambda_N$).

A low-order representation of the field $\mathbf{u}'_{LOM}(\mathbf{x}, t)$ can be created using an expansion of the first N_l POD modes associated with coherent dynamics in equation (6) thus yielding the coherent velocity field (Rowley, 2005; Noack *et al.*, 2011; Bourgeois *et al.*, 2013).

In developing a low-order representation, an additional filtering operation was carried out in order to separate modes containing predominately low-frequency spectral contributions associated with the slow-drift. These modes have characteristic time scales which are much longer than those associated with vortex shedding, or the cylinder displacement. It is thus beneficial to use a filtering operation aiming to improve the statistical convergence of the POD modes with time scales similar to the vortex shedding and cylinder motion. To extract the low-frequency contributions, the fluctuating velocity field $u'_i(\mathbf{x}, t)$ is low-pass filtered following the methodology employed by Riches *et al.* (2018). This results in both high and low frequency contributions to the coherent fluctuations.

For comparison with the POD method, phase-averaging was performed to calculate the coherent velocity field ($u_{ci}(\mathbf{x}, \theta)$) as a function of the phase angle as follows:

$$u_{ci}(\mathbf{x}, \theta) = \frac{1}{K} \sum_{n=0}^{K-1} u_i(\mathbf{x}, \left(\frac{\theta}{2\pi} + n \right) \frac{1}{f_{VS}}) \quad (9)$$

where K is the total number of PIV snapshots in each phase bin. The phase angle θ is defined following Perrin *et al.* (2007) as the angle between the two temporal coefficients of the POD mode pair associated with the primary vortex shedding in the wake

$$\theta = \tan^{-1} \left(\frac{a_2 / \sqrt{\lambda_2}}{a_1 / \sqrt{\lambda_1}} \right). \quad (10)$$

Alternatively, the wake can be phase-averaged to the cylinder position by calculating θ via the Hilbert transform of the cylinder position. A hybrid flow decomposition is proposed based on a combination of phase-averaging and POD. The new decomposition is derived by starting with the phase-averaged triple decomposition of equation (5), where $u_{ci}(\mathbf{x}, t)$ represents the phase-averaged contribution to the coherent velocity field given in equation (9). Next, the remaining incoherent velocity field (which still contains some coherent dynamics not captured through phase-averaging) is expanded using POD, yielding additional coherent dynamics of the residual velocity fluctuations. Thus, the triple decomposition becomes:

$$u_i(\mathbf{x}, t) = \underbrace{U_i(\mathbf{x})}_{Mean} + \underbrace{u_{ci}(\mathbf{x}, t) + u_{ci}''(\mathbf{x}, t)}_{Coherent} + \underbrace{u_i'''(\mathbf{x}, t)}_{Incoherent}. \quad (11)$$

where $u_{ci}''(\mathbf{x}, t)$ represents the POD contribution in the residual field. $u_i'''(\mathbf{x}, t)$ represents the remaining incoherent field.

RESULTS

Figure 2 shows the amplitude and frequency response for each case investigated. The results show a system response which is consistent with that observed in the literature for low mass ratio systems (Sarpkaya, 2004), where distinct initial branch, upper branch, lower branch, and desynchronization regions can be identified.

Phase-averaged vorticity fields for each PIV case within the lower branch and desynchronization region are shown in Figure 3. The desynchronized feature of the wake in Figs. 3e-h can be seen as no coherent vorticity field exists in each of the images. Interestingly, each of the first three points in the desynchronization region exhibits a significant amplitude response ($A_{10}^* > 0.2$) in Figure 2a, and there is a significant peak in the corresponding spectra at both the 'lock-in' frequency and Strouhal frequency (Figure 2b at $U^* \approx 8 - 11$). This is confirmed through direct assessment of the PSDF of the cylinder displacement signal in the desynchronization region at $U^* \approx 9$.

To investigate the nature of any coherent motions in the wake produced by the cylinder oscillation and vortex shedding within the desynchronization region, a POD analysis was performed on the planar PIV data using the decomposition technique of Equation (11) and the results are shown in Figure 4. The spatial modes of the first mode pair shown in Figure 4 show excellent agreement with that found in the initial branch by Riches *et al.* (2018). Moreover, if POD analysis was carried out on the velocity field directly, it can be shown that the resulting spatial modes remain largely unchanged, but the dual-frequency nature of the wake reappears (not shown for brevity). This suggests that the initial phase-averaging operation on the desynchronized data operates as a spatial velocity field filter, separating out the effects of the cylinder motion from the primary vortex shedding. The second mode pair shown in Figure 4 contains significant energy concentration at the beat frequency ($f/f_N = 0.58$) and the corresponding spatial modes are very similar to that observed in the initial branch by Riches *et al.* (2018). The third mode pair contains energy at the cylinders lock-in frequency and vortex shedding frequency, and appears to account for intermittent behaviours in the wake. Based on the results presented thus far, it appears as though the dominant mode of vortex shedding in

the desynchronization region is a uniquely modulated form of 2S vortex shedding found in the initial branch.

The results of the POD analysis indicate that despite the complex waveform describing the position trajectory of the cylinder, periodic vortex shedding occurs at the Strouhal frequency. This confirms that the dominant coherent structures are not synchronized to the cylinder motion in this branch. Given that the first mode pair extracted from POD primarily represents the vortices in the wake, the temporal evolution of this mode pair can be used in conjunction with the cylinder position data to elucidate the nature of the cylinders excitation when the wake and cylinder motion are synchronized in phase. In fact, the third most energetic POD temporal coefficient, a_3 is directly correlated to the state of the excitation in the wake. In particular, when $a_3 > 0$ the wake dampens the cylinder motion and when $a_3 < 0$, the wake excites the cylinder motion (Figure 5).

Figure 6 shows vorticity field reconstructions of the raw, phase-averaged, POD-based, and combined POD and phase-average for cases when the vortex shedding excites (Figure 6a) and dampens (Figure 6b) the cylinder motion. In both cases, it can be seen that the phase-averaged field alone does not capture the vortex shedding in the wake while the POD-based reconstruction more accurately captures the coherent dynamics. Qualitatively assessing Figure 6, during the excitation state the vortices formed contain stronger concentrations of vorticity and the wake width increases owing to a momentary increase in the oscillation amplitude. The converse is true, with the damping state providing weaker concentrations of vorticity and a narrower wake.

CONCLUSIONS

The wake of a circular cylinder undergoing VIV in the lower branch and desynchronization regions was investigated using a cyber-physical apparatus coupled with time-resolved two-dimensional planar PIV measurements. Different methods of resolving coherent contributions to the velocity field were investigated.

In the desynchronization region, phase-averaging was found to provide no insight into the coherent motions generated by the presence of the cylinder and its motion. A POD analysis and low order model reconstruction has shown a distinct wake vortex shedding pattern generated in the cylinder wake which is not synchronized to the cylinders motion. However, the wake flow becomes periodically altered depending on whether the cylinder motion is being damped or excited by the state of the vortex shedding, and this is mathematically defined by the beat frequency between the cylinders oscillation frequency and the vortex shedding frequency.

REFERENCES

- Bourgeois, J. A., Noack, B. R. & Martinuzzi, R. J. 2013 Generalized phase average with applications to sensor-based flow estimation of the wall-mounted square cylinder wake. *Journal of Fluid Mechanics* **736**, 316–350.
- Brika, D. & Laneville, A. 1993 Vortex-induced vibrations of a long flexible circular cylinder. *Journal of Fluid Mechanics* **250**, 481–508.
- Feng, C.C. 1968 The measurement of vortex induced effects in flow past stationary and oscillating circular and d-

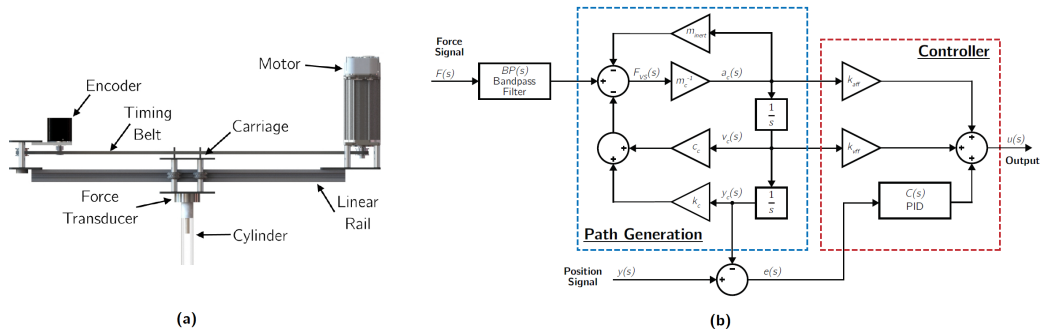


Figure 1. Experimental apparatus (a) and path generation algorithm (b) employed for all cyber-physical experiments. Additional details on this system can be found in (Riches & Morton, 2018).

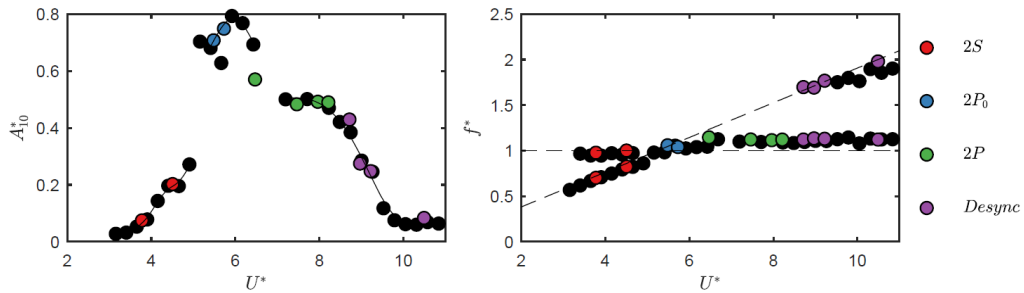


Figure 2. Amplitude and frequency response in the present study. Points are colored by the dominant vortex shedding mode obtained via phase-averaging. Black points correspond to cases where position and force data were recorded without PIV measurements.

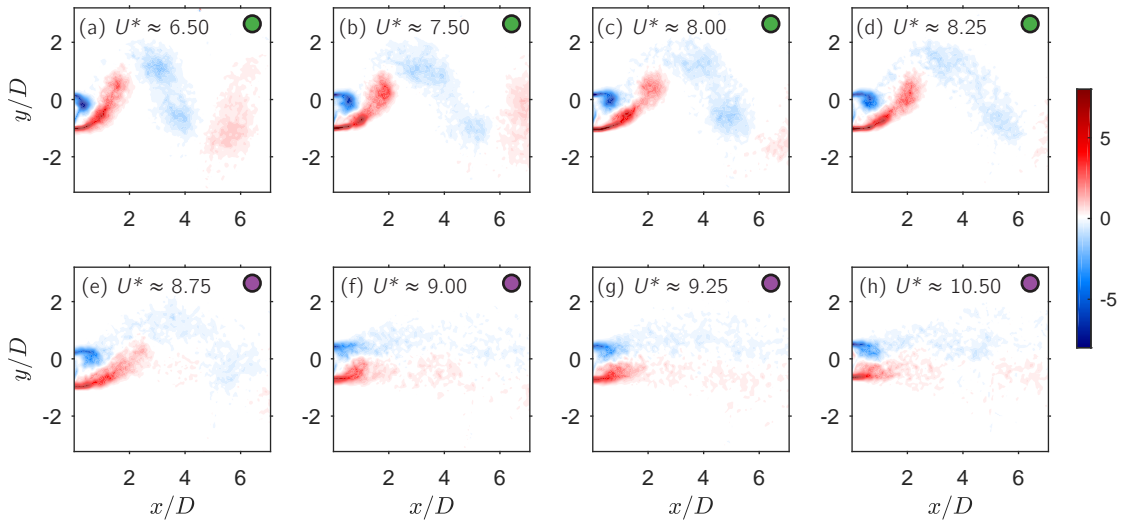


Figure 3. Phase-averaged vorticity fields for VIV. U^* increases from left-to-right top-to-bottom with the coloured markers corresponding to the primary wake mode according to the color coding in Figure 2. All images correspond to the same phase of the cylinder oscillation.

shaped bodies. Master's thesis, The University of British Columbia.
 Morse, T. L. & Williamson, C. H. K. 2009 Prediction of vortex-induced vibration response by employing controlled motion. *Journal of Fluid Mechanics* **634**, 5–39.
 Noack, Bernd R., Morzynski, Marek & Tadmor, Gilead 2011 *Reduced-Order Modelling for Flow Control*. SpringerWienNewYork.
 Perrin, P., Braza, M., Cid, E., Cazin, S., Barthet, A., Sevrain, A., Mockett, C. & Thiele, F. 2007 Obtaining

phase averaged turbulence properties in the near wake of a circular cylinder at high reynolds number using pod. *Experiments in Fluids* **43**, 341–355.
 Reynolds, W.C. & Hussain, A.K.M.F. 1972 The mechanics of an organized wave in turbulent shear flow. part 3. theoretical models and comparisons with experiments. *Journal of Fluid Mechanics* **54**, 263–288.
 Riches, G. 2018 Experimental investigation of vortex-induced vibrations using a cyber-physical system. PhD thesis, The University of Calgary.

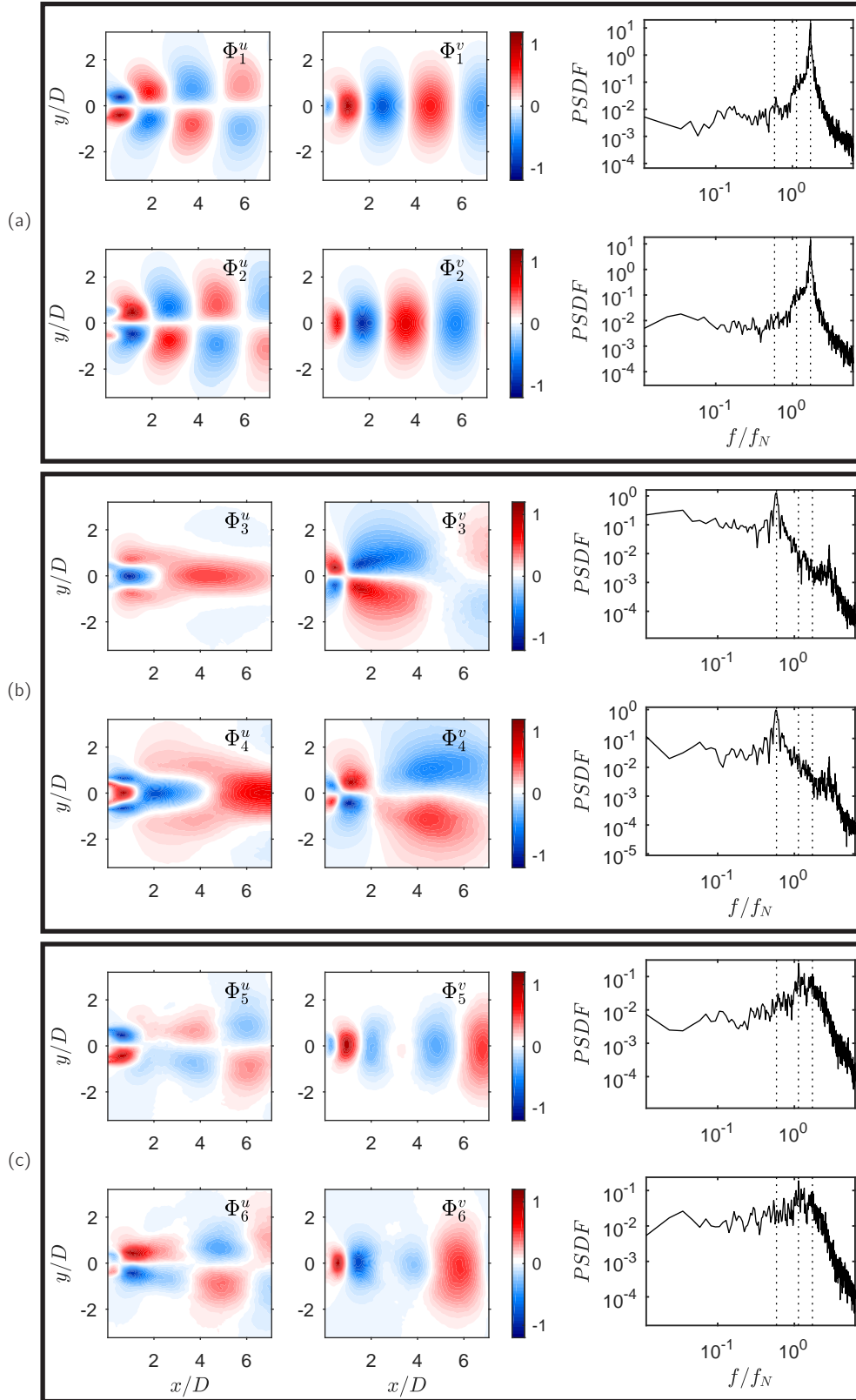


Figure 4. Spatial modes and temporal coefficient spectra for the identified coherent modes from the phase-averaged residual field at $U^* \approx 9.00$. From left to right, top to bottom: (a), Φ_1^u , Φ_1^v , PSDF of a_1 , Φ_2^u , Φ_2^v , PSDF of a_2 ; (b), Φ_3^u , Φ_3^v , PSDF of a_3 , Φ_4^u , Φ_4^v , PSDF of a_4 ; (c), Φ_5^u , Φ_5^v , PSDF of a_5 , Φ_6^u , Φ_6^v , PSDF of a_6 . All spatial modes are normalized by the peak value of the mode (i.e. $\Phi_i/\max(\Phi_i)$). The dashed lines in the spectra at $f/f_N = 0.58, 1.13, 1.72$ correspond to the beat frequency, first harmonic, and second harmonic, respectively.

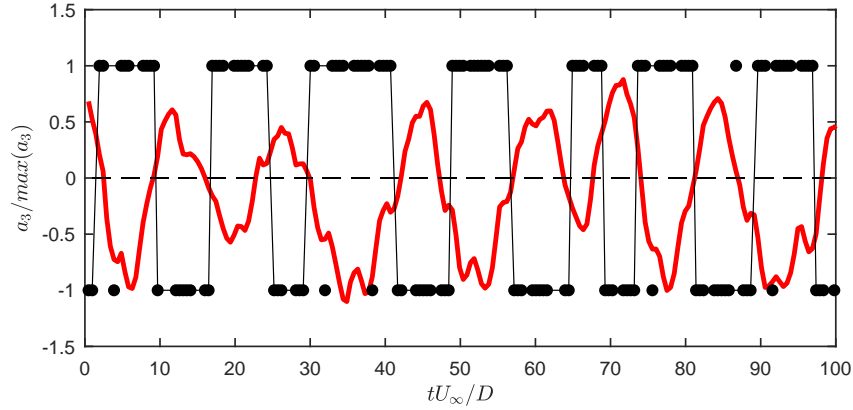


Figure 5. Normalized temporal coefficient a_3 associated with the beat frequency mode pair in red against the relative excitation state of wake on the cylinder motion in black. Values of $+1$ correspond to excitation, and values of -1 correspond to damping.

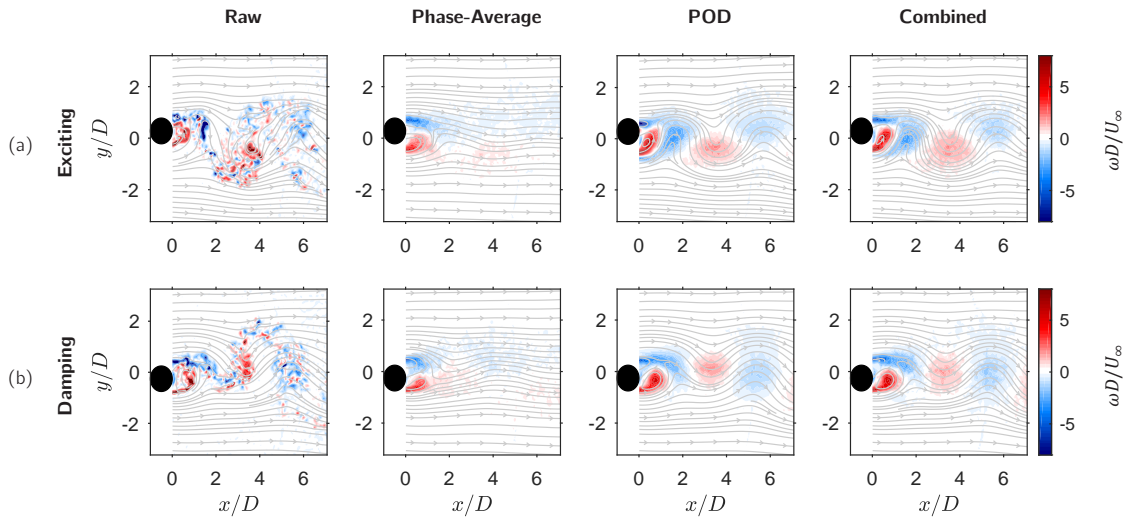


Figure 6. Vorticity field reconstructions (raw, phase-averaged, POD and combined method) for a case when the vortex shedding excites the cylinder motion (a) ($tU_\infty = 33.4$) and for a case when the vortex shedding damps the cylinder motion (b) ($tU_\infty = 44.6$). In (a), the cylinder is at its maximum positive displacement and in (b) it is at its maximum negative position. In both cases, the phase of the first mode pair is the same.

Riches, G., Martinuzzi, R. & Morton, C. 2018 Proper orthogonal decomposition analysis of a circular cylinder undergoing vortex-induced vibrations. *Physics of Fluids* **30**, 105103.
 Riches, G. & Morton, C. 2018 One-degree of freedom vortex-induced vibrations at constant reynolds number and mass-damping. *Experiments in Fluids* Accepted for Publication.
 Rowley, C W 2005 Model reduction for fluids , using bal-

anced proper orthogonal decomposition. *International Journal on Bifurcation and Chaos* **15** (3), 997–1013.
 Sarpkaya, T. 2004 A critical review of the intrinsic nature of vortex-induced vibrations. *Journal of Fluids and Structures* **19** (4), 389–447.
 Sirovich, L. 1987 Turbulence and the dynamics of coherent structures, part 1: Coherent structures. *Quarterly of Applied Mathematics* **45**, 561–571.